

SELF-SUPERVISED DOMAIN ADAPTATION FOR COMPUTER VISION TASKS

PREPRINT, COMPILED JUNE 6, 2022

Jiaolong Xu¹, Liang Xiao¹, and Antonio M. López²

¹Unmanned Systems Research Center, NIIDT, China

²Computer Vision Center, Universitat Autònoma de Barcelona, Spain

ABSTRACT

Recent progress of self-supervised visual representation learning has achieved remarkable success on many challenging computer vision benchmarks. However, whether these techniques can be used for domain adaptation has not been explored. In this work, we propose a generic method for self-supervised domain adaptation, using object recognition and semantic segmentation of urban scenes as use cases. Focusing on simple pretext/auxiliary tasks (e.g. image rotation prediction), we assess different learning strategies to improve domain adaptation effectiveness by self-supervision. Additionally, we propose two complementary strategies to further boost the domain adaptation accuracy within our method, consisting of prediction layer alignment and batch normalization calibration. For the experimental work, we focus on the relevant setting of training models using synthetic images, and adapting them to perform on real-world images. The obtained results show adaptation levels comparable to most studied domain adaptation methods, thus, bringing self-supervision as a new alternative for reaching domain adaptation. The code is available at <https://github.com/Jiaolong/self-supervised-da>.

Keywords Domain adaptation · Self-supervised learning · semantic segmentation · object recognition

1 INTRODUCTION

Since supervised (deep) machine learning became the key to solve computer vision tasks, the availability of task ground truth (*i.e.* supervision information) associated to the raw data (*i.e.* images and videos) has been a major practical problem. Training an image or video classifier requires to associate some class or attributes to the whole image/video [1, 2, 3, 4], training an object detector requires manual drawing of object bounding boxes [5, 6], training a CNN for semantic segmentation requires the delineation of the borders between the considered classes [7, 8], etc. This kind of ground truth (bounding boxes, class borders) is usually provided by human labeling, which is a costly process prone to errors due to subjectivity and fatigue. Therefore, procedures aiming at reducing human labeling became a research topic in itself too; or alternatively obtaining the most from a fixed budget for new labels. This underlying aim appears under different names depending on the practical situation at hand, *i.e.* the learning conditions. Under this umbrella we find concepts such as active learning, self-labeling, transfer learning, domain adaptation, and self-supervision.

In *active learning* [9, 10, 11], the learner receives a set of unlabeled data (images/videos) for training a visual accurate model, which must be done minimizing the labeling effort by choosing the best training data out of the total amount. This turns out into an iterative process where a human worker labels new automatically selected data in each cycle for model refinement. This contrasts with passive learning, where the training data is selected at random, eventually requiring more labeling budget.

In *self-labeling* [12, 13, 14], an initial visual model is trained on labeled data, after, the model is applied on unlabeled data to self-collect samples which are used then for refining the model by assuming that their label corresponds to the prediction of

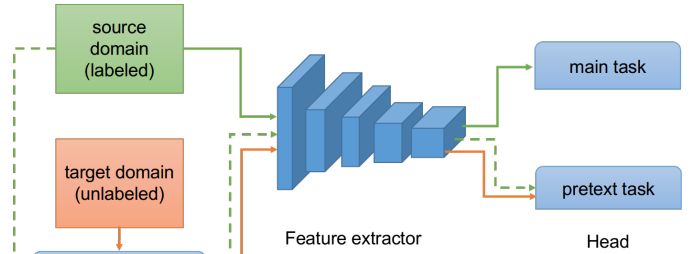


Figure 1: Proposed self-supervised domain adaptation framework. We learn a domain invariant feature representation by incorporating a pretext learning task which can automatically create labels from target domain images. The pretext and main task (e.g. object recognition or semantic segmentation) are learned jointly via multi-task learning. Solid lines indicate the forwarded data flow and the dash lines indicate optional data flow.

the model; turning out in an iterative process that must avoid drifting to systematic errors or easy samples.

In *transfer learning* [15, 16], a model is trained to perform a visual task (e.g. image classification) but aiming at reusing it to perform a new task (e.g. object detection) in a way that we minimize the amount of labeled data required to train for the new task (e.g. fine-tuning CNNs across tasks is a basic form of transfer learning).

In *domain adaptation* [17, 18, 19, 20], a model is trained to perform a visual task in a specific domain (e.g. semantic segmentation in synthetic images), however, we need to apply it to perform the same task in a correlated, but significantly different, domain (e.g. semantic segmentation in real-world images);

which is done by reusing the previous knowledge (in the form of model or labeled data) for minimizing the labeling effort in the new domain.

Finally, *self-supervised learning* [21, 22, 23] focuses on learning visual models without manual labeling; more specifically, auxiliary relatively simple tasks, known as *pretext tasks* in this context, are created for training a generic visual model in the form of CNN. The supervision consists in modifying the original visual data (e.g. a set of images) according to known transforms (e.g. image rotations [21]), training the pretext CNN to predict such transforms; thus, the transforms are the labels/supervision for the pretext task. This pretext CNN is then concatenated with another task-specific CNN. The former acting as generic feature extractor, and the later leveraging such features to create new ones specific for the *main task* of interest. Sometimes, both CNN blocks are fine-tuned [24], and sometimes the pretext CNN block is frozen and only the task-specific CNN block is fine-tuned [23]. Overall, the idea is that we can have a high number of supervised samples for the pretext task and this should compensate for a lower number of manually labeled samples for the main task.

Active learning can be naturally combined with transfer learning or domain adaptation [25]. Self-labeling can also be combined with transfer learning or domain adaptation [12]. Self-supervised learning, as usually performed, can be seen as a type of transfer learning (from the pretext task to the main task). What has not been explored, up to the best of our knowledge, is how self-supervised learning can support domain adaptation. This is the main focus of this paper, *i.e.* can we incorporate self-supervision to learn domain invariant feature representation? With this aim, we design a multi-task learning method to jointly train pretext and main tasks (Figure 1). The pretext task acts as nexus between source and target domains for learning a domain invariant feature representation for the main task. In this way, we have labels for the main task in source domain, but we do not require labels for such task in the target domain. In other words, via self-supervised learning, we perform unsupervised domain adaptation.

Accordingly, and using semantic segmentation of urban scenes as challenging main-task use case, the main contributions of this work are three-fold:

- We proposed a generic method for domain adaptation with self-supervised visual representation learning.
- Focusing on the image rotation prediction pretext learning task, we proposed several variations and studied their domain adaptation performance.
- We proposed additional strategies to further boost the self-supervised domain adaptation, including prediction layer alignment and batch normalization calibration.

This paper is organized as follows. In Section 2, we review related self-supervised representation learning and domain adaptation methods. In Section 3, we explain the proposed method. In Section 4, we conduct experiments on domain adaptation for object recognition as well as semantic segmentation, via our method. Finally, Section 5 summarizes the work and future directions.

2 RELATED WORK

Self-supervised visual representation learning An extensive review of deep learning-based self-supervised general visual feature learning methods from images or videos is provided in [26]. The recent work of self-supervised representation learning mainly focus on the design of pretext tasks. The work of [23] gives a comprehensive study of some state-of-the-art methods. A pretext task of predicting the relative location of image patches was first proposed in [27], where the patch ID is the supervision/label. This initial patch-based method has been followed by several variants [28, 22, 29]. Other works incorporate image colorization [30] or image inpainting [31] as pretext tasks. Yet other works focus on automatic ways of creating image samples with corresponding labels; for instance, in [24] the labels are classes derived from unsupervised image clustering, and in [21] the labels are image rotation angles since from an original image four possible rotations were created. As compared in [23], the rotation prediction based method [21] has shown promising results for learning high-level image representations. Therefore, in this work, we employ this pretext task as well as the location of image patches in line with [27]. In [32], relative depth prediction is used as a self-supervised proxy task, which has shown improvements to the downstream tasks, including semantic segmentation and car detection. However, it relies on the video data in order to obtain the relative depth.

Unsupervised Domain adaptation There have been numerous domain adaptation methods proposed for object recognition since [33]. After the pioneer work of [17, 18], semantic segmentation has also aroused increasing interests. Among existing domain adaptation methods, some try to align domains at input level, including GAN-based methods [34] and image stylization ones [35, 36, 37]. Some focus at feature level adaptation [17, 38, 39], and others on adapting the output space [40, 41, 42]. According to recent surveys [43, 20], most methods are built on the principle of domain adversarial training [44], with differences on how to incorporate it to the training of the segmentation network. Among the adaptation strategies we use as complement to self-supervision, the prediction layer alignment is similar to adversarial training for output space alignment.

In [14], iterative self-labeling and fine-tuning with spatial urban-scene location priors are used to perform the domain adaptation. In [18], a curriculum learning style is applied, where super-pixels are computed in source and target domains and their distributions must match as auxiliary task during semantic segmentation training. The use of such auxiliary task is similar in spirit to our multi-task learning approach with pretext tasks as nexus between source and target domains. However, neither our auxiliary tasks nor our complementary adaptation strategies are restricted to semantic segmentation, and they are way simpler than computing super-pixels. Comparing to these work, our method is not specifically designed for semantic segmentation but generic for various computer vision tasks.

In [45], the self-supervised learning method jigsaw puzzle is used for object recognition domain generalization and adaptation. As we will see in the experimental section, our method outperforms the jigsaw puzzle based method on both object recognition and semantic segmentation tasks. For semantic segmentation, we compare our results to [38, 18, 34, 35, 36, 37, 39,

42, 14]. The final semantic segmentation accuracy we obtain in target domain is superior to most of these methods, only behind [14] which is specific for semantic segmentation, and still not being far apart. Moreover, although it is out of the scope of this paper, our method can be complementary to some of the ones aforementioned, such as those based on adapting the input images via GANs.

3 METHOD

In this section, we first introduce our generic framework of self-supervised domain adaptation. Then, we present the considered pretext tasks. Finally, we introduce domain adaptation steps which complement self-supervision.

3.1 Self-supervised domain adaptation

3.1.1 Overview of the framework

Taking semantic segmentation as an example of main task, but without lose of generality, our method is shown in Figure 1; where E denotes an encoder network (feature extractor) and S a decoder network (specific of the main task), so that $E + S$ is a CNN for semantic segmentation. This CNN is trained end-to-end with source domain labeled samples, $\{X_s, Y_s\}$. We denote by P the network added to support the creation of a model for solving the pretext task. This model consists in the CNN $E + P$, where E is shared with the CNN of the main task. The pretext task training samples, $\{X_t, Y_t\}$, are automatically created from the target domain images so that the training of $E + P$ is also supervised.

The complete domain adaptation method is drawn in Algorithm 1, where we can see how the self-supervised domain adaptation is a joint training of models to perform the pretext and main tasks. During the forward propagation, both source and target domain samples pass through the shared encoder. After, the losses of the main task \mathcal{L}_{seg} and pretext task \mathcal{L}_p are computed, they are back-propagated and accumulated at the encoder. Because the encoder is trained with both source and target domain samples, it learns domain invariant feature representations. In the testing phase, we feed the target domain images to the encoder and pass the features to the decoder of the main task to obtain the predictions.

It is also possible to create pretext task samples with the source domain data, *i.e.*, dash lines in Figure 1. In this case, the pretext model can be trained with both source and target domain pretext task samples. We investigate this in Section 4.

3.1.2 Pretext tasks

In this section, we first introduce the image rotation prediction pretext task. Inspired by the image-patch based methods [27, 28, 22, 29], we also take into account the spatial layout of the image and propose a new pretext task.

Image rotation prediction as pretext task. We select image rotation prediction as pretext task due to its simplicity and superior performance on visual representation learning to other proposals [21]. Given a set of N_t training images from target domain $D_t = \{\mathbf{x}_i^t\}_{i=0}^{N_t}$, similar to [21], we define the set of geometric transformations as 2D image rotations by 0, 90, 180 and 270

Data: Labeled source domain images: $\{X_s, Y_s\}$, and unlabeled target domain images: $\{X_t\}$

Result: Model trained for main task in target domain

Create samples for pretext task: $\{X_t, Y_t\}$;

$i = 0$;

while $i < max_iters$ **do**

 Load target mini-batch $\{\mathbf{x}_i^t, \mathbf{y}_i^t\}$;

 Forward pass and compute \mathcal{L}_p ;

 Back-propagate \mathcal{L}_p gradients by P and E ;

 Update weights of P ;

 Load source mini-batch $\{\mathbf{x}_i^s, \mathbf{y}_i^s\}$;

 Forward pass and compute \mathcal{L}_{seg} ;

 Back-propagate \mathcal{L}_{seg} gradients by S ;

 Accumulate these gradients for E ;

 Update weights of E and S ;

end

Algorithm 1: Self-supervised domain adaptation

degrees. We denote the rotation function by $g(\mathbf{x}_i^t, r)$, $r \in [0, 3]$ rotates image \mathbf{x}_i^t by $r * 90$ degrees. The geometric transformation prediction model P takes feature map from E as input and outputs a probability distribution over all possible geometric transformations. The self-supervised training objective that the geometric transformation model must learn to solve is:

$$\min_{\theta_e, \theta_p} \frac{1}{N_t} \sum_{i=1}^{N_t} \mathcal{L}_p(\mathbf{x}_i^t, \theta_e, \theta_p), \quad (1)$$

where θ_e and θ_p are the parameters of the encoder E and pretext network P respectively, \mathcal{L}_p is the loss function defined as:

$$\mathcal{L}_p = -\frac{1}{4} \sum_{r=0}^3 \log(P(E(g(\mathbf{x}_i^t, r), \theta_e), \theta_p)). \quad (2)$$

By learning to predict the image orientations, the convolutional neural networks also implicitly learn to localize salient objects in the images, recognize their orientations and object types [21]. Such implicitly learned knowledge contains semantic information of the target domain images which is expected to improve the cross-domain feature representation power of the encoder network. In other words, the pretext task with target domain images helps the encoder to learn domain invariant feature representation, thus, helps to achieve domain adaptation.

The work of [21] uses full images from ImageNet [1]. However, the images from a specific domain are usually biased to particular structures or patterns, especially at a full image level. If we train a rotation prediction model with full images, the training process could find a trivial solution and, thus, not being able to learn a domain invariant feature representation. To avoid this problem, we first randomly crop an image patch from the full image and then rotate this patch. In this way, we create more difficult and diverse samples for the pretext task.

Spatial-aware rotation prediction as pretext task. Beyond image rotation, we further propose to take into account the image spatial layout to create a more complex pretext task. As depicted in Figure 2, instead of randomly cropping a patch from the full image, we first split the full image into four regions. From each region, we apply cropping and rotation operations as in

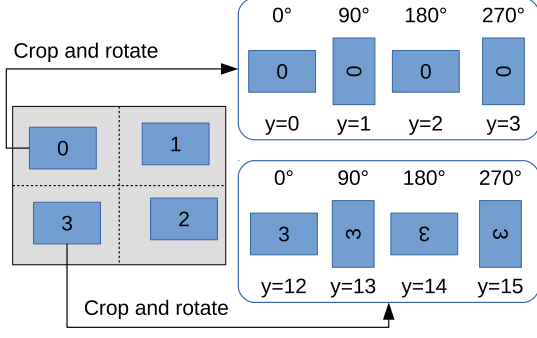


Figure 2: Region-based cropping and rotation.

the previous pretext task. We call this strategy spatial-aware rotation prediction. The dimension of a label is then extended from 4 (rotation angles) to 16 (spatial locations times rotation angles). This scheme encodes the geometry transform as well as spatial layout information, which results in a more complex pretext task.

3.1.3 Objective function for domain adaptation

Given a set of N_s labeled training images from the source domain $D_s = \{\mathbf{x}_i^s, \mathbf{y}_i^s\}_{i=0}^{N_s}$, the segmentation network takes as input the feature maps from $E(\mathbf{x}_i^s)$ and outputs the segmentation predictions: $\mathbf{O}_i^s = S(E(\mathbf{x}_i^s), \theta_e, \theta_s) \in \mathbb{R}^{H \times W \times C}$, where C is the number of semantic categories, H and W are the height and width of the output respectively, and θ_e and θ_s convey the parameters of E and S , respectively. The semantic segmentation training objective that we need to solve for E and S is:

$$\min_{\theta_e, \theta_s} \frac{1}{N_s} \sum_{i=1}^{N_s} \mathcal{L}_{seg}(\mathbf{x}_i^s, \theta_e, \theta_s), \quad (3)$$

where the segmentation loss is the cross-entropy loss, defined as:

$$\mathcal{L}_{seg} = - \sum_{h,w} \sum_{c \in C} \mathbf{y}_i^s(h, w, c) \log(\mathbf{O}_i^s(h, w, c)). \quad (4)$$

With Eq. (1) and Eq. (3), the objective function that self-supervised domain adaptation must solve is:

$$\min_{\theta_e, \theta_p, \theta_s} \frac{1}{N_s} \sum_{i=1}^{N_s} \mathcal{L}_{seg}(\mathbf{x}_i^s, \theta_e, \theta_s) + \frac{\lambda_p}{N_t} \sum_{j=1}^{N_t} \mathcal{L}_p(\mathbf{x}_j^t, \theta_e, \theta_p), \quad (5)$$

where λ_p is the weight to balance the two losses. In this work, we simply set $\lambda_p = 1$ for our experiments. The training process follows Algorithm 1.

3.2 Complementary adaptation steps

In this section, we introduce two different strategies to complement self-supervised domain adaptation, including adversarial training for prediction layer alignment and batch normalization.

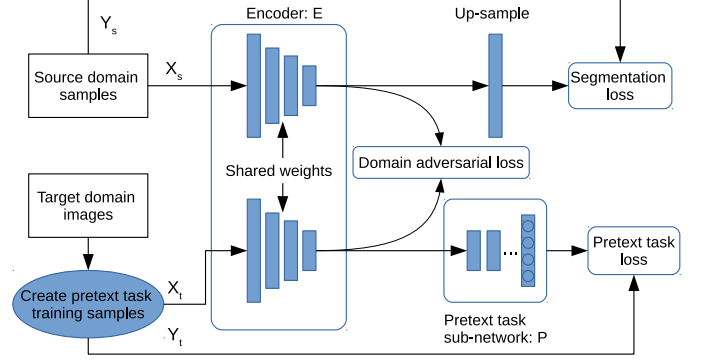


Figure 3: Self-supervised domain adaptation with prediction layer alignment.

3.2.1 Prediction layer alignment

The proposed pretext task learning is able to perform domain adaptation at feature level, however, the predicted semantic labels may still not be well aligned. There have been some previous work tackling this problem [42, 41]. In this work, we also consider to align the prediction layer to improve the domain adaptation performance. The main idea is illustrated in Figure 3. For semantic segmentation, we simplified the decoder by a single up-sampling layer. In this way, the last layer of the encoder is corresponding to the prediction layer. By placing a domain discriminator after the prediction layer, the commonly used domain adversarial training can be employed. We denote by D the discriminator and θ_d for its parameters. Given an input image \mathbf{x}_i , the discriminator takes as input the feature maps from the encoder $E(\mathbf{x}_i)$ and performs the binary classification to distinguish whether the feature map is from the source image or the target one, $\mathbf{Z}_i = D(E(\mathbf{x}_i))$, $\mathbf{Z}_i \in \mathbb{R}^{H \times W \times 2}$. The training of D is a standard supervised training, which minimizes the following 2-D cross-entropy loss:

$$\mathcal{L}_d(\mathbf{x}_i, \theta_d) = - \sum_{h,w} [(1-z) \log \mathbf{Z}_i(h, w, 0) + z \log \mathbf{Z}_i(h, w, 1)], \quad (6)$$

where h, w are indexing the output layer, $z = 0$ indicates that the sample is drawn from the target domain, and $z = 1$ if it is drawn from the source domain.

In order to learn a domain invariant feature representation, we want the encoder to *fool* the domain discriminator D , which is equivalent to minimize the following adversarial loss function:

$$\mathcal{L}_{adv}(\mathbf{x}_i, \theta_e) = - \sum_{h,w} [(1-z) \log \mathbf{Z}_i(h, w, 1) + z \log \mathbf{Z}_i(h, w, 0)]. \quad (7)$$

Combining the self-supervised domain adaptation objective function Eq. (5), the overall optimization problem that we solve

is as following:

$$\begin{aligned}
\min_{\theta_e, \theta_p, \theta_s, \theta_d} & \frac{1}{N_s} \sum_{i=1}^{N_s} \mathcal{L}_{seg}(\mathbf{x}_i^s, \theta_e, \theta_s) \\
& + \frac{\lambda_p}{N_t} \sum_{i=1}^{N_t} \mathcal{L}_p(\mathbf{x}_i^t, \theta_e, \theta_p) \\
& + \frac{\lambda_{adv}}{N_t + N_s} \sum_{i=1}^{N_t + N_s} \mathcal{L}_{adv}(\mathbf{x}_i, \theta_e) \\
& + \frac{\lambda_d}{N_t + N_s} \sum_{i=1}^{N_t + N_s} \mathcal{L}_d(\mathbf{x}_i, \theta_d), \quad (8)
\end{aligned}$$

where λ_{adv} and λ_d are the weights to balance the corresponding losses. In this work, we set $\lambda_{adv} = 0.01$ and $\lambda_d = 1.0$ for our experiments. We show how this prediction layer alignment improves the self-supervised domain adaptation in Section 4.3.5.

3.2.2 Batch normalization calibration

The batch normalization (BN) is originally designed to reduce the internal covariate shift and speedup the training of deep neural networks. Given a mini-batch $\mathcal{B} = \{\mathbf{z}_{1..m}\}$ as input, BN layer first calculates the mean and variance by $\mu_{\mathcal{B}} = \frac{1}{m} \sum_{i=1}^m \mathbf{z}_i$, $\sigma^2 = \frac{1}{m} \sum_{i=1}^m (\mathbf{z}_i - \mu_{\mathcal{B}})^2$. Each example is then normalized by $\hat{\mathbf{z}}_i = \frac{\mathbf{z}_i - \mu_{\mathcal{B}}}{\sqrt{\sigma^2 + \epsilon}}$, where ϵ is a constant added to the mini-batch variance for numerical stability. The normalized values are then scaled and shifted by $\lambda \hat{\mathbf{z}}_i + \beta$ to produce the output, where λ and β are learnable parameters.

For a trained source domain model, $\mu_{\mathcal{B}}$ and σ^2 are statistics from source domain images, which may cause domain shift when applied with target domain images. What we proposed in this work is to re-calibrate these statistics to reduce the domain shift. Given a pretrained network, we keep all the learnable parameters fixed and feed forward the target domain training images. During this forward propagation, we re-calculate the mean and variation values of each BN layer.

Our BN calibration is similar to the AdaBN method [46]. However, AdaBN adopts an online algorithm to estimate the mean and variance, while we simply use the common moving average mean and variance available in existing deep learning frameworks. AdaBN is applied at the inference stage, *i.e.* to the testing images, while we use BN calibration as a post training process with target domain training images.

4 EXPERIMENTS AND RESULTS

In this section, we conduct experiments to validate the proposed domain adaptation method for both object recognition and semantic segmentation.

4.1 Implementation Details

We implement the proposed method using the PyTorch framework on a single GTX 1080 Ti GPU with 11 GB memory. For object recognition, we use the code base of JiGen [45]². We use

Method	art paint.	cartoon	sketches	photo	Avg.
SRC[50]	74.70	72.40	60.10	92.90	75.03
Dial[51]	87.30	85.50	66.80	97.00	84.15
DDiscovery[50]	87.70	86.90	69.60	97.00	85.30
SRC[45]	77.85	74.86	67.74	95.73	79.05
JiGen[45]	84.88	81.07	79.05	97.96	85.74
Ours(SRC)	79.33	76.75	64.40	96.39	79.22
Ours(Jigsaw)	84.93	83.85	69.04	93.92	82.94
Ours(Rot)	89.35	84.14	79.54	98.24	87.82

Table 1: Multi-source Domain Adaptation results on PACS (ResNet-18). Three domains are used as source datasets and the remaining one as target.

the default hyper-parameters and ResNet-18 architecture. The deep networks used in our semantic segmentation experiments are ResNet-101 based DeepLab-v2 [47] and dilated residual networks (DRN) [48]. Specifically, we take the commonly used DRN-26 architecture in order to compare to other state-of-the-art methods. Both networks are initialized with ImageNet [1] pretrained weights.

4.2 Domain adaptation for object recognition

For object recognition, we evaluate on the multiple source domain adaptation dataset PACS [49], which has 7 object categories and 4 domains (Photo, Art Paintings, Cartoon and Sketches). Figure 4 shows sample images from PACS dataset. We follow the same experimental settings as [45] and trained our model considering three domains as source datasets and the remaining one as target. Following [45], we also compare to the domain discovery method DDiscovery [50] and Dial [51]. We set three different random seeds and run each experiment three times. The final result is the average over the three repetitions. To make a fair comparison, we run jigsaw puzzle method with the same random seeds and denoted by Ours(jigsaw). The results are shown in Table 1. Our image rotation based self-supervised domain adaptation outperforms all baselines.

4.3 Domain adaptation for semantic segmentation

For semantic segmentation, we adapt semantic segmentation models from the source domain of synthetic images to the target domain of real-world images. For the synthetic datasets, we use SYNTHIA [52] and GTA5 [53], and for the target domain, we use the Cityscapes dataset [7]. The GTA5 [53] dataset is rendered from the Grand Theft Auto V video game. It consists of 24996 images with resolution of 1914×1052 and has 19 classes compatible with Cityscapes dataset. We use the full set of GTA5 as our source domain training set. For SYNTHIA dataset, we use the SYNTHIA-RAND-CITYSCAPES set [52] as the source domain training set, which contains 9400 images. We evaluate with the 16 common classes for SYNTHIA to Cityscapes domain adaptation. The training set of Cityscapes has 2975 images which are used as unlabeled target domain training samples. The validation set of Cityscapes has 500 samples which are used as our testing set.

We conduct ablation studies to understand the impact of each component of our self-supervised domain adaptation. If not otherwise specified, all the experiments in this section use ResNet-101 as backbone network and the domain adaptation is from GTA5 to Cityscapes.

²<https://github.com/fmcarlucci/JiGenDG>

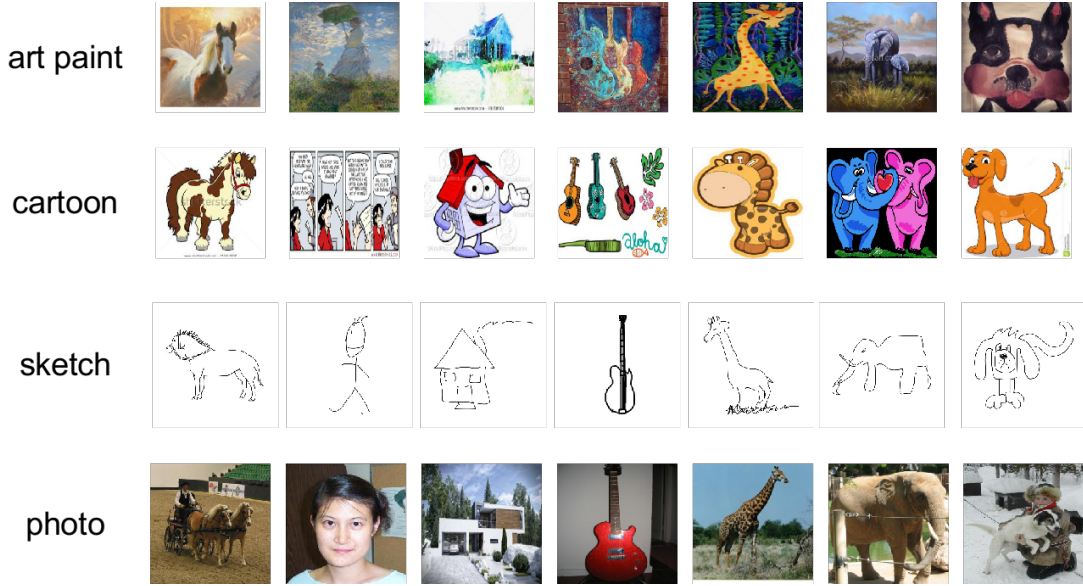


Figure 4: Sample images from PACS dataset. Each row represents a domain and each column represents a category.

4.3.1 Pretext task learning strategies

As discussed in Section 3.1.1, source domain training samples can also be used in pretext task learning together with the target domain samples. We denote by **MixRot** this scheme and by **Rot** the pretext task learning with target domain training samples only. The first two rows in Table 2 show their domain adaptation results. As can be seen from Table 2, mixing source domain training data in the pretext learning shows even inferior results, which may be because the mixed samples make the model more source domain oriented and reduces domain invariant representation power.

Next, we would like to know whether the proposed spatial-aware rotation prediction pretext task is better than the simple rotation prediction strategy, *i.e.*, the **Rot** method. Table 2 displays the results of the spatial-aware rotation prediction pretext task as **SPRot**. It turns out that the more difficult pretext task learning leads to worse domain adaptation performance. In our practice, the pretext task learning of **SPRot** has more difficulties to converge than **Rot**, and this may result in the failure of learning good feature representations. Therefore, how to design a proper pretext task for domain adaptation still needs more exploration.

We also compare our method **Rot** to the jigsaw puzzle based self-supervision [45]. The results are shown in Table 3, where SYN2CS denotes SYNTHIA to Cityscapes domain adaptation and GTA2CS for GTA5 to Cityscapes. **Rot** outperforms the jigsaw puzzle for both SYN2CS and GTS2CS. Especially for GTA2CS, jigsaw puzzle has shown very limited gain (1.2 percentage point) while **Rot** still achieved 6.2 percentage point.

4.3.2 Input image size for pretext task learning

As the images from Cityscapes dataset have large resolution (*e.g.*, 1024×2048). We are interested in what cropping size is best for the self-supervised learning. In Table 2, we compare three different cropping sizes. The smallest cropping size (128×128) shows worst performance due to too small field of view to learn good representations. Comparing the remaining two cropping

sizes, we see that the larger one (400×400) does not further improve the performance. In fact, when we use the full image as input, the pretext learning easily gets stuck in a trivial solution, *i.e.* 100% prediction accuracy. As a result, the final model fails to perform domain adaptation. Thus, we believe that a proper cropping size is important to control the difficulty of learning pretext tasks.

4.3.3 Feature extraction layer

By default, the pretext task takes as input the features extracted from the last layer of the encoder. However, whether the last layer is the best for domain adaptation is unclear. In this section, we train self-supervised domain adaption models with different feature extraction layers. We mainly compare the feature extraction from the middle and the end of the encoder. Table 2 shows the corresponding results, where **Middle** represents the feature extraction from middle layer and **Final** uses features from the end layer of the encoder. As, in this case, the decoder of the segmentation network is simply an up-sampling layer without any learnable parameter, the **Final** layer is actually the prediction layer of the segmentation network. As we can see from the results, the model **Middle** shows slightly better results and we think the pretext task learning is not very sensitive to the choice of feature extraction layers.

4.3.4 Performance correlation between pretext task learning and domain adaptation

In many domain adaptation applications, we may not have access to the target domain labels for validation. We were wondering whether the accuracy of the pretext task can be used as indicator of the accuracy of the domain adaptation. Therefore, it is interesting to know whether the accuracy on pretext task can be used as a proxy for the accuracy on the main task at the target domain. Figure 5 depicts the accuracy of pretext task vs. domain adaptation (in the semantic segmentation task). The different dot colors just correspond to different network architectures (ResNet-101

GTA5 → Cityscapes																				
	mIoU	road	sidewalk	building	wall	fence	pole	light	sign	veg	terrain	sky	person	rider	car	truck	bus	train	mbike	bike
Rot	41.2	87.6	25.7	77.5	19.8	16.8	29.0	32.1	20.5	79.9	32.9	75.3	58.2	26.0	79.0	23.3	31.6	2.1	26.9	37.7
MixRot	40.3	79.4	13.7	77.6	20.1	19.4	27.9	36.3	30.6	83.3	29.2	74.4	60.2	29.2	64.9	27.8	18.1	0.3	28.4	44.2
SPRot	37.7	80.6	19.2	76.1	17.8	16.0	29.4	32.9	20.2	77.5	19.6	74.2	59.0	28.1	67.8	31.2	12.4	0.4	26.8	25.9
128x128	38.6	77.8	13.5	78.9	18.6	19.1	25.8	34.3	28.8	77.4	19.2	72.1	60.2	27.3	67.0	31.5	8.3	0.7	32.1	40.7
256x256	41.2	87.6	25.7	77.5	19.8	16.8	29.0	32.1	20.5	79.9	32.9	75.3	58.2	26.0	79.0	23.3	31.6	2.1	26.9	37.7
400x400	40.3	79.4	13.7	77.6	20.1	19.4	27.9	36.3	30.6	83.3	29.2	74.4	60.2	29.2	64.9	27.8	18.1	0.3	28.4	44.2
Middle	41.2	87.6	25.7	77.5	19.8	16.8	29.0	32.1	20.5	79.9	32.9	75.3	58.2	26.0	79.0	23.3	31.6	2.1	26.9	37.7
Final	40.4	84.1	25.0	79.5	15.5	15.5	29.5	30.5	27.8	82.1	21.7	80.3	54.3	26.0	70.1	29.5	29.2	0.2	26.3	40.9

Table 2: Domain adaptation performance under different pretext task settings (ResNet-101).

Method	SYN2CS			GTA2CS		
	SRC	Adapt	Gain	SRC	Adapt	Gain
Jigsaw puzzle	30.5	34.3	3.8	35.0	36.2	1.2
Ours(Rot)	30.5	36.1	5.6	35.0	41.2	6.2

Table 3: Comparison with jigsaw puzzle method (ResNet-101).

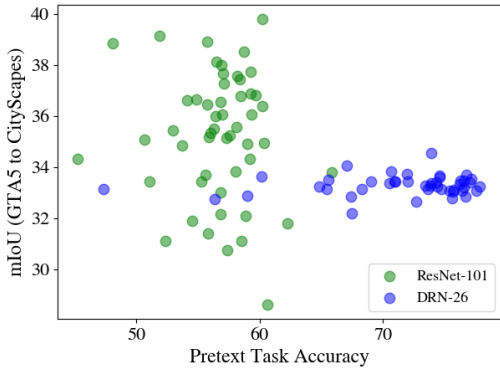


Figure 5: Performance correlation between pretext task learning and domain adaptation. The different dot colors just correspond to different network architectures (ResNet-101 green, DRN-26 blue).

green, DRN-26 blue). Given one color, the different dots are obtained from the validation set, *i.e.* we recorded the mIoU and pretext task accuracy on validation set at intermediate iterations of the training phase.

For a fixed model architecture, the best performing domain adaptation model does have relatively higher accuracy on pretext task, but the best pretext task accuracy does not indicate best domain adaptation model. We believe that how to design a pretext task to reliably estimate the accuracy of the main task in the target domain is an interesting and challenging future work.

4.3.5 Evaluation of complementary strategies

Table 4 shows the results with different complementary strategies. The source domain model is denoted by **SRC** and the model trained with target domain samples is denoted by **TAR**, which represent the lower and upper bound of the accuracy respectively. **Rot** is our baseline method. **+Adv** is with prediction layer alignment (Section 3.2.1), which improves **Rot** by 1.1 percentage points. **+BN** is with BN calibration (Section 3.2.2), which does not show improvement over **Rot**. But when com-

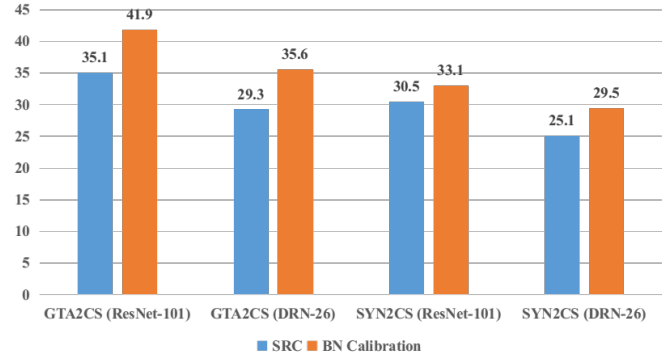


Figure 6: Domain adaptation performance of BN calibration. The vertical axis denotes mIoU accuracy.

bined **Adv** and **BN**, we obtain the best results, improving **Rot** by 2.1 percentage points. Table 5 shows more results with other architectures and datasets, where **+Adv** has consistent improvements to **Rot** but **+Adv+BN** gets saturated for the SYN2CS problem.

To understand why BN does not have consistent improvements, we further conduct experiments using only BN calibration for domain adaptation. Figure 6 shows the results on multiple datasets using multiple networks. BN calibration alone achieves surprisingly good results, and the best domain adaptation gain even reaches 6.8 percentage points. However, when combined with **Rot** or **Rot+Adv**, it only improves 1 or 2 percentage points. This might be because **Rot** and **Rot+Adv** have already learned domain invariant representation that effectively reduces the covariate shift and BN calibration could not contribute more to the adapted model. The reason that **Adv** gives consistent rise to the base method is because **Adv** further aligns the predicted label distributions which is more complementary adaptation to the **Rot** than the provided by **BN**.

4.4 Comparison to the state-of-the-art

Lastly, we compare our method to some recently published state-of-the-art works which use similar architectures to ours. The results are shown in Table 5. The compared methods cover large varieties of domain adaptation mechanisms, including input/feature/output level alignment methods, curriculum and self-labeling based methods. Some of these methods are also surveyed in [43]. We refer the readers to [43] for more details. The results in Table 5 show that our adapted models (**Adapt**)

GTA5 → Cityscapes																				
	mIoU	road	sidewalk	building	wall	fence	pole	light	sign	veg	terrain	sky	person	rider	car	truck	bus	train	mbike	bike
Rot	41.2	87.6	25.7	77.5	19.8	16.8	29.0	32.1	20.5	79.9	32.9	75.3	58.2	26.0	79.0	23.3	31.6	2.1	26.9	37.7
+Adv	42.3	84.9	31.9	80.4	19.0	21.7	28.2	34.7	27.7	82.8	26.5	72.7	58.2	25.3	82.1	18.7	42.1	1.2	26.0	39.7
+BN	41.0	86.7	32.6	78.7	20.4	20.6	27.0	28.6	15.8	82.4	38.0	74.6	57.6	24.0	80.1	23.6	29.3	0.8	23.2	34.8
+Adv+BN	43.3	87.3	35.0	80.0	20.2	21.8	28.7	32.3	25.8	83.3	29.3	73.7	58.7	25.7	83.2	27.5	43.6	1.8	27.5	38.1
SRC	35.0	77.5	12.3	71.3	8.1	18.8	26.6	32.4	19.6	73.7	11.3	67.9	55.2	24.3	73.3	16.9	9.9	0.9	26.4	39.5
TAR	65.3	96.5	74.3	88.0	48.8	41.2	42.3	47.0	60.7	88.5	52.8	90.5	68.6	48.9	91.1	68.5	69.5	46.3	51.3	65.0

Table 4: Evaluation of complementary strategies (ResNet-101).

Method	Network	SYN2CS			GTA2CS			Mechanism
		SRC	Adapt	Gain	SRC	Adapt	Gain	
CyCADA[34]	DRN-26	-	-	-	21.7	39.5	17.8	Input adversary
Stylization[35]	DRN-26	22.0	35.0	13.0	22.9	38.3	15.4	Input stylization
DCAN[36]	ResNet-101	28.0	36.5	8.5	29.8	38.5	8.7	Input stylization
FCAN[37]	ResNet-101	-	-	-	29.2	46.6	17.4	Input stylization + feature adversary
ADR [38]	ResNet-50	-	-	-	25.3	33.3	8.0	Feature adversary
GAM[39]	DRN-26	-	-	-	-	40.2	-	Feature adversary
AdaptSegNet[42]	ResNet-101	-	-	-	36.6	41.4	4.8	Output adversary
CBST[14]	ResNet-38	29.2	42.5	13.3	35.4	47.0	11.6	Self-labelling
CURC[18]	DRN-26	21.9	28.2	6.3	-	-	-	Curriculum
Ours(Rot)	ResNet-101	30.5	36.1	5.6	35.0	41.2	6.2	Self-supervision
	DRN-26	25.1	28.9	3.8	29.4	34.6	5.2	
Ours(Rot+Adv)	ResNet-101	30.5	39.3	8.8	35.0	42.3	7.3	Self-supervision + output adversary
	DRN-26	25.1	31.7	6.6	29.4	36.1	6.7	
Ours(Rot+Adv+BN)	ResNet-101	30.5	38.8	8.3	35.0	43.3	8.3	Self-supervision + output adversary + BN
	DRN-26	25.1	30.4	5.3	29.4	36.2	6.8	

Table 5: Comparison with the state-of-the-art methods. The result of AdaptSegNet [42] here is from the single resolution version as our output adversarial method is built on top of this version.

achieve comparable accuracies to the state-of-the-art. It is worth noting some of these state-of-the-art methods obtain worse results than we obtain when training with the source data alone (SRC columns), so their relative gain is higher. Looking at the absolute accuracy (Adapt columns) of the best performing architectures (*i.e.*, ResNet based ones), only CBST is better than ours in SYN2CS and GTA2CS, and FCAN in GTA2CS. On the other hand, with this work we aim at encouraging the use of pretext tasks for domain adaption of semantic segmentation models, which, as mentioned before, can be a complementary idea to others. We also find that a deeper network (ResNet-101) can achieve better domain adaptation gain than the shallow one (DRN-26). The only method that outperforms ours systematically is CBST, which is specifically designed for semantic segmentation on urban scenarios. Our pretext tasks and complementary adaptation methods are generic.

5 CONCLUSION

In this work, we have explored self-supervised learning for domain adaptation. We have shown that a simple image rotation prediction (pretext task) self-supervision can achieve state-of-the-art domain adaptation performance. We have studied several pretext tasks as well as complementary domain adaptation strategies. Taking object recognition and semantic segmentation of urban scenes as relevant use cases, we have performed an ablative analysis of the different components included in our overall domain adaptation procedure. This analysis reveals that self-supervision and prediction layer alignment are systematically complementary. As future work, we would like to investigate more pretext tasks and to apply our method to other relevant vision tasks.

ACKNOWLEDGEMENTS

This work is supported by the National Natural Science Foundation of China (NSFC, NO. 61601508, 61790565 and 61803380). Antonio M. López acknowledges the financial support by the Spanish project TIN2017-88709-R (MINECO/AEI/FEDER, UE), as well as the financial support by ICREA under the ICREA Academia Program. Antonio also thanks the Generalitat de Catalunya CERCA Program and its ACCIO agency.

REFERENCES

- [1] J. Deng, W. Dong, R. Socher, L.-J. Li, K. Li, and L. Fei-Fei. Imagenet: A large-scale hierarchical image database. In *CVPR*, Miami, Florida, US, 2009.
- [2] H. Kuehne, H.-H. Jhuang, E. Garrote-Contreras, T. Poggio, and T. Serre. HMDB: a large video database for human motion recognition. In *ICCV*, 2011.
- [3] Alex Krizhevsky, Ilya Sutskever, and Geoffrey E Hinton. Imagenet classification with deep convolutional neural networks. In *NIPS*, Lake Tahoe, Nevada, USA, 2012.
- [4] K. Soomro, A.-R. Zamir, and M. Shah. UCF101: A dataset of 101 human actions classes from videos in the wild. *arXiv preprint arXiv:1212.0402*, 2012.
- [5] M. Everingham, L. Van Gool, C.K.I. Williams, J. Winn, and A. Zisserman. The PASCAL visual object classes (VOC) challenge. *IJCV*, 88(2):303–338, 2010.
- [6] Tsung-Yi Lin, Michael Maire, Serge Belongie, James Hays, Pietro Perona, Deva Ramanan, Piotr Dollár, and C Lawrence Zitnick. Microsoft coco: Common objects in context. In *ECCV*, 2014.

- [7] Marius Cordts, Mohamed Omran, Sebastian Ramos, Timo Rehfeld, Markus Enzweiler, Rodrigo Benenson, Uwe Franke, Stefan Roth, and Bernt Schiele. The cityscapes dataset for semantic urban scene understanding. In *CVPR*, 2016.
- [8] Gerhard Neuhold, Tobias Ollmann, Samuel Rota Bulò, and Peter Kotschieder. The mapillary vistas dataset for semantic understanding of street scenes. In *ICCV*, 2017.
- [9] Y. Abramson and Y. Freund. SEmi-automatic VISual LEarning (SEVILLE): a tutorial on active learning for visual object recognition. In *CVPR*, 2005.
- [10] Burr Settles. Active learning. *Synthesis Lectures on Artificial Intelligence and Machine Learning*, 6(1):1–114, 2012.
- [11] Soumya Roy, Asim Unmesh, and Vinay P. Namboodiri. Deep active learning for object detection. In *BMVC*, 2018.
- [12] J. Xu, S. Ramos, D. Vázquez, and A.M. López. Domain adaptation of deformable part-based models. *T-PAMI*, 36(12):2367–2380, 2014.
- [13] Jiaolong Xu, D. Vázquez, Krystian Mikolajczyk, and A.M. López. Hierarchical online domain adaptation of deformable part-based models. In *ICRA*, 2016.
- [14] Yang Zou, Zhiding Yu, BVK Vijaya Kumar, and Jinsong Wang. Unsupervised domain adaptation for semantic segmentation via class-balanced self-training. In *ECCV*, 2018.
- [15] S.J. Pan and Q. Yang. A survey on transfer learning. *T-KDE*, 22(10):1345–1359, 2009.
- [16] Ross B. Girshick, Jeff Donahue, Trevor Darrell, and Jitendra Malik. Rich feature hierarchies for accurate object detection and semantic segmentation. In *CVPR*, Columbus, Ohio, USA, 2014.
- [17] Judy Hoffman, Dequan Wang, Fisher Yu, and Trevor Darrell. Fcns in the wild: Pixel-level adversarial and constraint-based adaptation. In *CVPR*, 2016.
- [18] Yang Zhang, Philip David, and Boqing Gong. Curriculum domain adaptation for semantic segmentation of urban scenes. In *ICCV*, 2017.
- [19] Yuhua Chen, Wen Li, Christos Sakaridis, Dengxin Dai, and Luc Van Gool. Domain adaptive faster r-cnn for object detection in the wild. In *CVPR*, 2018.
- [20] Mei Wang and Weihong Deng. Deep visual domain adaptation: A survey. *Neurocomputing*, 2018.
- [21] Spyros Gidaris, Praveer Singh, and Nikos Komodakis. Unsupervised representation learning by predicting image rotations. In *ICLR*, 2018.
- [22] Dahun Kim, Donghyeon Cho, Donggeun Yoo, and In So Kweon. Learning image representations by completing damaged jigsaw puzzles. In *WACV*, 2018.
- [23] Alexander Kolesnikov, Xiaohua Zhai, and Lucas Beyer. Revisiting self-supervised visual representation learning. *arXiv preprint arXiv:1901.09005*, 2019.
- [24] Mathilde Caron, Piotr Bojanowski, Armand Joulin, and Matthijs Douze. Deep clustering for unsupervised learning of visual features. In *ECCV*, 2018.
- [25] D. Vázquez, A.M. López, J. Marín, D. Ponsa, and D. Gerónimo. Virtual and real world adaptation for pedestrian detection. *T-PAMI*, 36(4):797–809, 2014.
- [26] Longlong Jing and Yingli Tian. Self-supervised visual feature learning with deep neural networks: A survey. *arXiv preprint arXiv:1902.06162*, 2019.
- [27] Carl Doersch, Abhinav Gupta, and Alexei A Efros. Unsupervised visual representation learning by context prediction. In *ICCV*, 2015.
- [28] Mehdi Noroozi and Paolo Favaro. Unsupervised learning of visual representations by solving jigsaw puzzles. In *ECCV*, 2016.
- [29] T Nathan Mundhenk, Daniel Ho, and Barry Y Chen. Improvements to context based self-supervised learning. In *CVPR*, 2018.
- [30] Richard Zhang, Phillip Isola, and Alexei A Efros. Colorful image colorization. In *ECCV*, 2016.
- [31] Deepak Pathak, Philipp Krahenbuhl, Jeff Donahue, Trevor Darrell, and Alexei A Efros. Context encoders: Feature learning by inpainting. In *CVPR*, 2016.
- [32] Huaizu Jiang, Gustav Larsson, Michael Maire, Greg Shakhnarovich, and Erik Learned-Miller. Self-supervised relative depth learning for urban scene understanding. In *ECCV*, 2018.
- [33] K. Saenko, B. Hulis, M. Fritz, and T. Darrell. Adapting visual category models to new domains. In *ECCV*, 2010.
- [34] Judy Hoffman, Eric Tzeng, Taesung Park, Jun-Yan Zhu, Phillip Isola, Kate Saenko, Alexei A. Efros, and Trevor Darrell. Cycada: Cycle consistent adversarial domain adaptation. In *ICML*, 2018.
- [35] Aysegul Dundar, Ming-Yu Liu, Ting-Chun Wang, John Zedlewski, and Jan Kautz. Domain stylization: A strong, simple baseline for synthetic to real image domain adaptation. *arXiv preprint arXiv:1807.09384*, 2018.
- [36] Zuxuan Wu, Xintong Han, Yen-Liang Lin, Mustafa Gokhan Uzunbas, Tom Goldstein, Ser Nam Lim, and Larry S Davis. Dcan: Dual channel-wise alignment networks for unsupervised scene adaptation. In *ECCV*, 2018.
- [37] Yiheng Zhang, Zhaofan Qiu, Ting Yao, Dong Liu, and Tao Mei. Fully convolutional adaptation networks for semantic segmentation. In *CVPR*, 2018.
- [38] Kuniaki Saito, Yoshitaka Ushiku, Tatsuya Harada, and Kate Saenko. Adversarial dropout regularization. In *ICLR*, 2018.
- [39] Haoshuo Huang, Qixing Huang, and Philipp Krähenbühl. Domain transfer through deep activation matching. In *ECCV*, 2018.
- [40] Kuniaki Saito, Kohei Watanabe, Yoshitaka Ushiku, and Tatsuya Harada. Maximum classifier discrepancy for unsupervised domain adaptation. In *CVPR*, 2018.
- [41] Jeroen Manders, Elena Marchiori, and Twan van Laarhoven. Simple domain adaptation with class prediction uncertainty alignment. In *ICML*, 2018.
- [42] Y.-H. Tsai, W.-C. Hung, S. Schuster, K. Sohn, M.-H. Yang, and M. Chandraker. Learning to adapt structured output space for semantic segmentation. In *CVPR*, 2018.

- [43] Yang Zhang, Philip David, Hassan Foroosh, and Boqing Gong. A curriculum domain adaptation approach to the semantic segmentation of urban scenes. *arXiv preprint arXiv:1812.09953*, 2018.
- [44] Yaroslav Gani, Evgeniya Ustinova, Hana Ajakan, Pascal Germain, Hugo Larochelle, François Laviolette, Mario Marchand, and Victor Lempitsky. Domain-Adversarial Training of Neural Networks. In *ICML*, 2015.
- [45] Fabio M Carlucci, Antonio D’Innocente, Silvia Bucci, Barbara Caputo, and Tatiana Tommasi. Domain generalization by solving jigsaw puzzles. In *CVPR*, 2019.
- [46] Yanghao Li, Naiyan Wang, Jianping Shi, Jiaying Liu, and Xiaodi Hou. Revisiting batch normalization for practical domain adaptation. *PR*, 2018.
- [47] Liang-Chieh Chen, George Papandreou, Iasonas Kokkinos, Kevin Murphy, and Alan L Yuille. Deeplab: Semantic image segmentation with deep convolutional nets, atrous convolution, and fully connected crfs. *T-PAMI*, 40(4):834–848, 2018.
- [48] Fisher Yu, Vladlen Koltun, and Thomas Funkhouser. Dilated residual networks. In *CVPR*, 2017.
- [49] Da Li, Yongxin Yang, Yi-Zhe Song, and Timothy M Hospedales. Deeper, broader and artier domain generalization. In *ICCV*, 2017.
- [50] Massimiliano Mancini, Lorenzo Porzi, Samuel RotaBulo, Barbara Caputo, and Elisa Ricci. Boosting domain adaptation by discovering latent domains. In *CVPR*, 2018.
- [51] Fabio Maria Carlucci, Lorenzo Porzi, Barbara Caputo, Elisa Ricci, and Samuel Rota Bulo. Just dial: Domain alignment layers for unsupervised domain adaptation. In *International Conference on Image Analysis and Processing*, 2017.
- [52] German Ros, Laura Sellart, Joanna Materzynska, David Vázquez, and Antonio López. The SYNTHIA Dataset: A large collection of synthetic images for semantic segmentation of urban scenes. In *CVPR*, 2016.
- [53] Stefan Roth, Stephan Richter, Vibhav Vineet and Vladlen Koltun. Playing for data: Ground truth from computer games. In *ECCV*, 2016.